

Theoretical Analysis of the Electronic Properties of N3 Derivatives

Maamar Rekhis,[†] Frédéric Labat,[‡] Ourida Ouamerli,[†] Ilaria Ciofini,[‡] and Carlo Adamo^{*,‡}

Laboratoire de Physico-chimie Quantique, Institut de Chimie, Université des Sciences et de la Technologie Houari Boumediene, BP 32, El-Alia, 16111 Bab-Ezzouar, Alger, Algeria, and Laboratoire d'Electrochimie et de Chimie Analytique, CNRS UMR-7575, Ecole Nationale Supérieure de Chimie de Paris, 11 rue Pierre et Marie Curie, F-75231 Paris Cedex 05, France

Received: July 17, 2007; In Final Form: September 22, 2007

The structural and electronic properties of nine derivatives of the N3 complex (*cis*-[Ru(4,4'-COOH-2,2'-bpy)₂(NCS)₂]) have been studied, using density functional theory (DFT) at a hybrid (PBE0) level, with the aim of finding a systematic way to improve their spectral absorption in the visible region for photoelectrochemical applications. To this end, by means of time dependent-DFT (TD-DFT) calculations, excited states were investigated in solution to simulate UV–vis spectra. Several effects have been taken into account: the effect of the presence and deprotonation of the carboxylic groups as well as the variation of the chalcogen within the NCX ligand (X = S, Se, or Te). Besides the excellent agreement between theoretical and available experimental data, with regards to potential future experimental applications of the investigated complexes, from the calculations, the *cis*-Ru(dcbpyH₂)(NCSe)₂ may appear as a good candidate to enhance the response of the N3 dye to light, even if only slightly.

1. Introduction

Conversion of sunlight into electrical energy, through photoelectrochemical solar cells, has attracted much attention during the last years. Indeed, while several semiconductor systems have been employed in the direct conversion of solar energy into chemical or electrical energy for years now,¹ only recently a major development has been made with the introduction of the third generation of cells, based, for example, on dye-sensitized nanostructured mesoporous TiO₂ thin films.²

To date, the most efficient sensitizers used are those based on polypyridine complexes of d⁶ transition metal ions, such as Ru(II), Os(II), or Re(I).³ Metal-to-ligand charge transfers (MLCT), corresponding to promotion of an electron from a molecular orbital (MO) that is largely metal based (t_{2g} filled states) to a MO that is largely ligand based (empty π* bipyridine states), account for nearly all of the visible light absorption of these complexes. Hence, the smaller is the gap, the more red-shifted is the MLCT transition.

Despite the vivid activity devoted to the design of new photosensitizers,⁴ the most effective sensitizer is still the so-called N3 dye *cis*-[Ru(4,4'-COOH-2,2'-bpy)₂(NCS)₂], referred to as *cis*-[Ru(dcbpyH₂)(NCS)₂] in the following (bpy = 2,2'-bipyridine), already introduced in the early 1990s.⁵ In fact, this latter sensitizer presents a broad light absorption in the visible range, relatively long-lived excited states, as well as high thermal stability. In addition, its acidic carboxylic groups allow for a firm adsorption on the semiconductor. Despite its unmatched performances, it presents some drawbacks because its absorption coefficients and incident monochromatic photon-to-current efficiency (IPCE) strongly decrease at longer wavelengths (i.e., above 600 nm). Furthermore, combined to the triiodide/iodide couple in the electrolyte, a mismatch between the redox level of the latter couple and that of the ground state of the N3 dye

appears, the regeneration of the dye (carried out by the couple) thus being the main loss factor in these dye-sensitized solar cells.⁶

To red-shift the MLCT transitions of this latter complex, one of the possibilities is to tune the coordination shell of the central metal ion, filling it with mono-, bi-, as well as tridentate ligands in mixed fashions.⁴ More precisely, the basic idea is to reduce MLCT transition energies either by tuning the metal-based MO (t_{2g} tuning) or by tuning the polypyridine acceptor-based MO (π* tuning). Unfortunately, so far, most attempts have failed,⁷ except for the “black dye” (tri(cyanato)-2,2'2''-terpyridyl-4,4',4''-tricarboxylate)Ru(II), which introduced a new efficiency record in 2001,⁸ photoconversion spectrum of systems based on this sensitizer reaching about 100 nm further into the red or IR region as compared to those based on N3 or its deprotonated forms.^{5,9} Recently however, the N3 dye combined to guanidinium thiocyanate in the electrolyte has outcome the performances of this latter sensitizer with a new record conversion efficiency of 11.04%.⁶ Thus, the performances of N3 still remain unmatched.

A possible interesting alternative to red-shift MLCT transitions while keeping most of the N3 features would be to tune the NCS ligand to modify the electron density at the metal center, which largely determines the t_{2g} energy levels. In particular, to the best of our knowledge, no attempts have been made to replace S by isoelectronic elements such as Se or Te in the N3 complex to tune the t_{2g} levels if one excepts the experimental work of Kohle and collaborators on the Ru-(bmipy)(dcbpy)NCSe complex.⁷

In this context, we investigate at the ab initio level the related selenium- and tellurium-based compounds of the N3 dye, that is, systems where the NCSe and NCTe forms of the ambidentate NCX ligand of the N3 dye are taken into account.

To this end, density functional theory (DFT) and time-dependent DFT (TD-DFT) have been respectively used to describe the electronic and structural properties, as well as the UV–vis spectra of the complexes. In particular, a computational

* Corresponding author. E-mail: carlo-adamo@enscp.fr.

[†] Université des Sciences et de la Technologie Houari Boumediene.

[‡] Ecole Nationale Supérieure de Chimie de Paris.

TABLE 1: Selected Computed Structural Parameters of *cis*-[Ru(L)₂(NCX)₂] Derivatives (PBE0 Level in Gas Phase) as a Function of the Ligand (L = bpy, dcbyH₂) and the Chalcogen (X = S, Se, or Te) in Comparison with Available Experimental and Theoretical Structures (Distances in Å, Angles in deg; For Labeling, Refer to Figure 1)

L	bpy				dcbyH ₂				dcby ²⁻				
	X	S	S ^{exp,a}	Se	Te	S	S ^b	Se	Te	S	S ^b	S ^{exp,c}	Se
RuN ₃	2.047	2.051	2.048	2.051	2.042	2.065	2.043	2.046	2.067	2.091	2.013(14)–2.030(13)	2.068	2.071
RuN ₈	2.040	2.041	2.042	2.043	2.034	2.057	2.035	2.037	2.054	2.077	2.036(15)–2.058(12)	2.056	2.057
RuN ₁₄	2.033	2.055	2.028	2.030	2.023	2.046	2.020	2.020	2.065	2.100	2.046(16)–2.048(12)	2.059	2.057
N ₃ C ₂	1.370	1.351	1.370	1.370	1.372		1.373	1.373	1.373		1.383(18)–1.440(24)	1.373	1.373
N ₃ C ₄	1.356	1.340	1.356	1.356	1.357		1.357	1.357	1.357		1.351(26)–1.353(19)	1.357	1.356
N ₈ C ₇	1.374	1.349	1.373	1.373	1.375		1.375	1.374	1.375		1.288(23)–1.379(20)	1.374	1.374
N ₈ C ₉	1.357	1.348	1.356	1.356	1.359		1.359	1.358	1.357		1.337(21)–1.338(18)	1.357	1.357
C ₂ C ₇	1.466	1.452	1.467	1.467	1.465		1.465	1.465	1.472		1.449(21)–1.487(19)	1.472	1.472
N ₁₄ C ₁₅	1.193	1.124	1.192	1.190	1.194	1.197	1.193	1.191	1.188	1.191	1.103(27)–1.162(21)	1.187	1.186
C ₁₅ X ₁₆	1.669	1.654	1.803	2.008	1.664	1.671	1.797	2.002	1.693	1.702	1.615(18)–1.685(22)	1.828	2.034
RuN ₃ C ₂	115.6	115.6	115.6	115.4	115.4		115.4	115.5	116.1		115.3(9)–117.4(10)	116.1	116.0
RuN ₃ C ₄	124.4	125.3	124.4	124.6	124.6		124.7	124.8	124.9		125.4(10)–127.3(13)	124.9	125.0
RuN ₈ C ₇	115.6	115.5	115.5	115.5	115.5		115.4	115.3	116.3		114.5(9)–116.2(10)	116.3	116.2
RuN ₈ C ₉	125.4	125.5	125.3	125.3	125.4		125.5	125.3	125.0		123.3(13)–125.0(11)	125.0	125.0
RuN ₁₄ C ₁₅	175.3	168.2	173.7	173.0	178.0		176.3	174.6	176.4		168.9(12)–178.0(17)	176.4	176.9
N ₈ RuN ₃	99.4	96.4	99.2	99.3	99.1		98.9	98.7	97.7		95.9(5)–97.8(5)	97.5	97.3
N ₈ RuN ₈	93.7	90.7	93.6	94.5	93.4		93.3	92.9	92.2		90.6(5)	91.8	91.5
N ₃ RuN ₈	79.3	78.7	79.3	79.3	79.6		79.6	79.5	78.6		79.1(5)–79.8(5)	78.6	78.6
N ₃ C ₂ C ₇ N ₈	−1.5	~6	−1.4	−1.3	−1.4		−0.9	−1.1	0.4		−0.6 to 1.0	0.4	0.3

^a See ref 31. ^b B3LYP/LanL2DZ, see ref 32. ^c See ref 33.

protocol shown to be particularly effective both for the calculation of electronic structure properties at molecular and solid-state level and for the prediction of excited-state properties using a TD-DFT approach has been applied.^{10–15} This method relies on the use of a relatively small basis set (and pseudo potential for the heavier atoms) in conjunction with a hybrid functional (PBE0), which has been shown to be particularly efficient for the calculation of valence excitations of similar Ru and Os compounds,^{10,12} of fully organic dyes,^{16–18} and even of Rydberg states, provided that a larger basis is used.¹⁹ Furthermore, to simulate bulk solvatochromic effects on UV–vis spectra, a simple but effective approach, such as the continuum model of the solvent of Miertus, Scrocco, and Tomasi (the polarizable continuum model, PCM²⁰), proven reliable for similar systems,^{21,22} has been applied.

Using this protocol, the effect of the different chemical functionalizations will be separately analyzed. First, the role of the carboxylic groups on the bidentate bpy-type ligands on the overall structural and electronic properties of the N3 dye will be investigated by comparing the properties of the *cis*-[Ru(bpy)₂(NCS)₂] and the *cis*-[Ru(dcbyH₂)₂(NCS)₂] complexes. Next, the effect of the deprotonation of the N3 dye will also be accounted for by studying the N3⁴⁻ form of the dye (L = dcby²⁻; X = S) as well as its selenium- and tellurium-related compounds (X = Se, Te). Finally, vertical excitation energies will be computed for all species, compared to each other, and checked against experimental data, when available.

Our results allow one to separately understand the role of each functionalization by analyzing its effect on the MO energy levels as well as on the overall macroscopic properties (such as the UV–vis spectra) and could be used to design new N3-based ligands, besides the obvious synthetic and stability problems not taken into account in this contribution.

2. Computational Details

All calculations have been performed with the Gaussian 03 code²³ at the hybrid DFT level in the gas phase as well as in solution. More precisely, the PBE0²⁴ hybrid exchange correlation functional, casting 25% of exact HF exchange into the PBE exchange and correlation functional,²⁵ has been used throughout. This hybrid functional has been chosen due to its nonempirical

nature and because it has proven to give reliable results in the prediction of molecular structures and properties of complex systems containing Ru and Os atoms.^{10,12,26} Full structural optimizations have been carried out without any symmetry constraints in the gas phase because previous calculations on similar systems showed that solvent effects are small on geometrical parameters.²¹ The nature of each stationary point has then been verified by harmonic vibrational frequency calculations.

In terms of basis sets, the double- ξ quality, Hay and Wadt (LanL2DZ) basis sets²⁷ have been used for all atoms, with the corresponding effective core potentials²⁸ applied for ruthenium, sulfur, selenium, and tellurium atoms.

To compute the UV–vis transition of selected Ru-based compounds, the time-dependent DFT approach²⁹ has been used at the same level of theory. Only singlet–singlet transitions, that is, spin-allowed transitions, have been taken into account. Moreover, only transitions with non-negligible oscillator strengths ($f \geq 0.02$) are reported and discussed. Computations were carried out to cover a spectral region up to 350 nm for all systems under investigation, that is, to span the whole UV–vis spectral domain. From these calculations, two quantities, related to the UV–vis spectra, are readily available: the energy of any electronic E_{n-m}^{00} transition and the corresponding oscillator strength (f). On the basis of these quantities, the spectra were afterwards simulated, using Gaussian functions, to have a direct comparison with the experimental data and get the absorption maxima. A full-width at half-maximum (fwhm), that is, the broadening of each peak (individual transition), of 0.15 eV was applied. Solvent effects have been taken into account by an implicit model, the polarizable continuum model (PCM) of Tomasi et al.²⁰ using the structure optimized in the gas phase. More precisely, the conductor-like PCM model, as implemented in Gaussian 03 (CPCM),^{23,30} has been used throughout, and water was considered as solvent.

3. Ground-State Structural and Electronic Properties

Table 1 summarizes the selected geometrical parameters of the fully optimized structures obtained for all systems in the gas phase. The corresponding labeling scheme is given in Figure

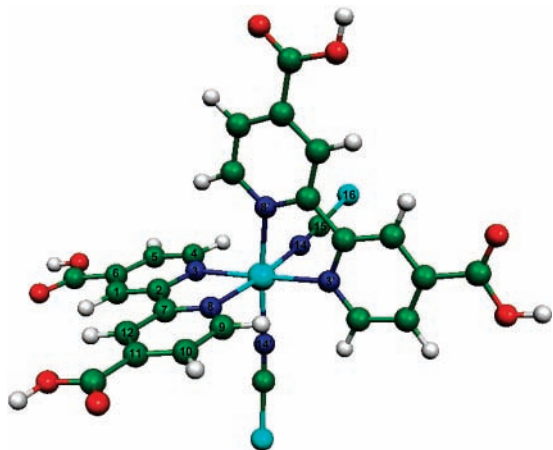


Figure 1. Schematic structure and labeling scheme of the *cis*-Ru^{II}-(dcbpyH₂)₂(NCX)₂ complex (X = S, Se, or Te). Nearly symmetrically related atoms, due to the approximate C₂ axis, are labeled with slanted primes.

1. As a general rule, we refer to the various complexes investigated as *cis*-Ru(L)₂(NCX)₂ (L = bpy, dcbpy; X = S, Se, or Te).

It should be noticed that all complexes under investigation show an almost symmetric arrangement of the ligands, due to an approximate C₂ axis along the bisectors of the N₈'-Ru-N₈ and N₁₄'-Ru-N₁₄' angles (refer to Figure 1), but, no matter which NCX or L ligand is chosen, the Ru coordination is far from being octahedral due to the different nature of the two ligands.

However, while computed structures are very close to being symmetric (for instance, symmetrically related bond lengths are within 0.001 Å of each other), the experimental structure of [*cis*-Ru(dcbpy)₂(NCS)₂]⁴⁻³³ is far from being symmetric, due mainly to crystal packing effects. For this reason, while the computed geometrical data reported in the tables correspond to averaged values between symmetry-related moieties, two different values are given in the case of the experimental data, if available. Moreover, following experimental evidence,^{5,33-35} ambidentate NCX ligands are considered N-bonded to the Ru atom.

We can first note that, no matter which L ligand is taken into account, reported bond lengths and angles are highly similar for all complexes. The carboxylic groups, either in their protonated or in their deprotonated forms, thus have an overall small influence on computed structural parameters. This is especially true for the bpy cores, for which this influence is found negligible. The only parameters significantly affected by the tuning of L are the Ru-N distances. Indeed, while these distances are almost the same for the complexes containing bpy and dcbpyH₂ as ligand, a significant increase is observed when going from the protonated form of the carboxylated ligand (dcbpyH₂) to the corresponding deprotonated one (dcbpy²⁻). This behavior can be related to the higher π-acceptor character of dcbpy²⁻ with respect both to bpy and dcbpyH₂ having similar π-acceptor characters and to the reduced back-donation from the metal orbitals to the ligand π* orbitals due to the energy rise of the bipyridine-based LUMOs in N₃⁴⁻. Therefore, we can conclude that bpy-, dcbpyH₂-, and dcbpy²⁻-based complexes are not significantly different, at least from a structural point of view.

When tuning the NCX ligand, that is, when going from X = S to X = Se or Te, the same conclusions hold. No significant difference on the Ru coordination sphere can be noticed. Clearly,

the only sizable difference between the three systems is related to the C₁₅X₁₆ bond length (refer to Figure 1), which strongly increases when going from a thiocyanate ligand to a seleno- or tellurocyanate one. This is related to the more diffuse character of the orbitals of the selenium and tellurium atoms, as compared to the sulfur ones, that is, to a larger “atomic” radius of the atoms while descending in the same group. Furthermore, on passing from NCS, NCSe, to NCTe, the spatial extent of the p orbitals of C and of X atoms strongly differs, and the p-p hybridization therefore decreases, leading to significantly higher C-X bond lengths.

In conclusion, the computed data suggest that the close environment of the Ru atom is not significantly perturbed by the nature of the chalcogen atom of the NCS ligand and by the functionalization/deprotonation of the bpy-type ligand.

Finally, it is worth mentioning that computed data are in excellent agreement with available X-ray structure and in line with previous theoretical works (see Table 1). Indeed, it is noteworthy that computed Ru-N distances are closer to experimental values than previously reported B3LYP/LanL2DZ data (see ref 32). Therefore, the PBE0 functional seems to correct the well-known overestimated picture of Ru-N distances given by the B3LYP functional in these types of complexes^{22,32,36-39} and further confirms the validity of our computational approach.

For what concerns the effect of functionalization on electronic structure, the molecular orbital energy level diagrams for all investigated structures in solution are given in Figure 2. Here, we essentially comment on the ground-state electronic structures computed in solution, because solvent effects have already been shown to be mandatory to correctly describe the orbital splitting in the case of the deprotonated form of the bare L ligand.⁴⁰

As previously pointed out by De Angelis et al. for the carboxylated S-based complexes (see, for instance, ref 32), the HOMO, HOMO-1, and HOMO-2 orbitals correspond to an antibonding interaction between Ru t_{2g}, X_p, and nitrogen lone pairs of the NCX ligands (referred to as t_{2g}-π* in Figure 2), while the HOMO-3 results from a nonbonding combination of an X lone pair and a nitrogen p orbital located on the NCX ligand, for all complexes. In both the S- and the Se-based structures, the bonding counterparts of the three HOMO, HOMO-1, and HOMO-2 orbitals (referred to as t_{2g}-π in the diagram) are then found lower in energy in case of the neutral species. For the deprotonated complex, however, these states are much lower in energy and are thus not represented in Figure 2. Finally, π bpy states are located below -0.25 au for all complexes no matter which L or X ligand is taken into account. We should note here that, in case of the Te-based compounds, the t_{2g}-π levels are not found and are, instead, replaced by t_{2g}-π* ones. This is related to the highly diffuse character of the p orbitals of Te, vanishing the p-p hybridization between C and X atoms observed with the NCS and NCSe ligands. Moreover, we note that almost exclusively carboxylate-based states are found between the HOMO-4 and the π bpy states for the N₃⁴⁻ complex. In the neutral species, these states lie much lower in energy. Finally, the LUMOs are essentially π* MO localized on the bpy moiety.

From an energetic point of view, we note that, no matter which L ligand is taken into account, similar trends are obtained when going from NCS to NCSe and NCTe, that is, slight destabilization of the HOMO and stabilization of the LUMO, resulting in a gap lowering when going from S to Se and Te as reported in Table 2. Furthermore, solvation widens the gap. For example, the 3.06 eV HOMO-LUMO gap of N₃⁴⁻ in the gas phase is increased to 3.25 eV in solution. This is in line with a

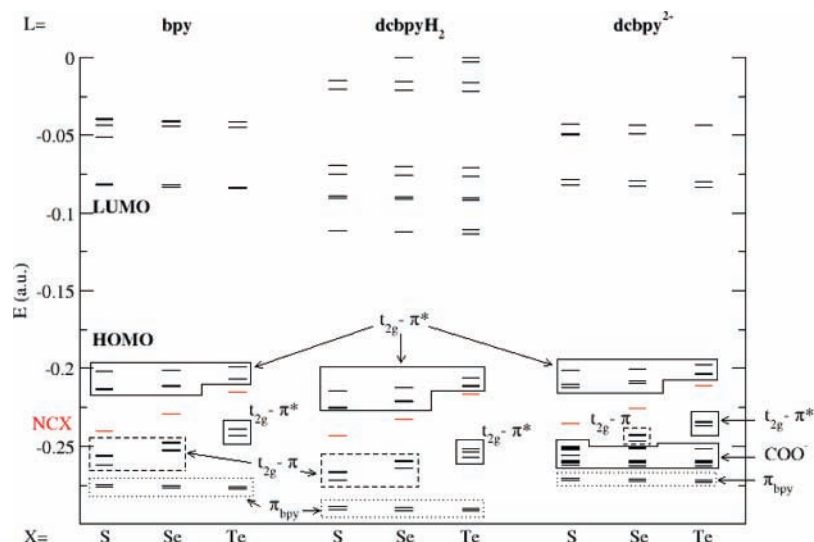


Figure 2. Energy level diagram (E in au) of the *cis*-[Ru(L)₂(NCX)₂] complexes investigated as computed in solution. Bonding and antibonding levels are in black. Nonbonding levels are in red.

TABLE 2: Computed Energies of Frontier Orbitals and Associated HOMO–LUMO Gap (in au) of *cis*-[Ru(L)₂(NCX)₂] Derivatives (L = bpy, dcbpy; X = S, Se, or Te) in the Gas Phase^a

	bpy			dcbpyH ₂			dcbpy ²⁻		
	S	Se	Te	S	Se	Te	S	Se	Te
HOMO	-0.175 (-0.202)	-0.169 (-0.201)	-0.161 (-0.199)	-0.194 (-0.214)	-0.188 (-0.212)	-0.178 (-0.206)	0.107 (-0.201)	0.105 (-0.200)	0.102 (-0.197)
LUMO	-0.096 (-0.082)	-0.097 (-0.083)	-0.099 (-0.084)	-0.129 (-0.111)	-0.129 (-0.112)	-0.131 (-0.113)	0.219 (-0.082)	0.217 (-0.082)	0.213 (-0.083)
gap	0.079 (0.120)	0.071 (0.118)	0.061 (0.115)	0.065 (0.103)	0.058 (0.100)	0.047 (0.092)	0.113 (0.120)	0.112 (0.118)	0.111 (0.114)

^a Corresponding values computed in solution are reported in parentheses.

previous theoretical work.³² Finally, we mention that the widening of the gap is more pronounced for the Se- and Te-based compounds than for the S compounds. This effect is related to the softer character of Se and Te, that is, to the higher polarizability of the former atoms, as compared to S. Thus, it is not surprising that Se and Te complexes will be more affected by solvation.

In general, from the analysis of the orbital splitting it is evident that the energy levels of Ru centered t_{2g} orbitals are only slightly affected by the nature of the chalcogen, a sizable difference being noticed only when passing to Te. Furthermore, the gap computed for Ru(bpy)₂(NCX)₂ compounds is very similar to that of corresponding Ru(dcbpyH₂)(NCX)₂ complexes, thus showing that the carboxylic groups do not affect the near Fermi level splitting. Indeed, deprotonation of Ru(dcbpyH₂)₂(NCX)₂ strongly destabilizes the LUMO and opens the gap.

4. Excited-State Properties: The Calculation of UV–Vis Spectra

Before starting the discussion concerning the UV–vis spectra of the different species in detail, it is worthwhile to make some general comments, because the same overall conclusions hold for all systems. In all cases, in the energy range investigated, two bands clearly appear. While the first one (around 500 nm) convolutes multiple MLCT transitions corresponding to one-electron excitations from $t_{2g}-\pi^*/t_{2g}-\pi$ to π^*-bpy levels, the second one (around 370 nm) has a mixed character. Indeed, in this latter case, in addition to multiple MLCT transitions, ligand-based charge transfer (LBCT) transitions between NCX nonbonding levels and π^*-bpy MOs appear.

TABLE 3: Selected Vertical Excitation Energies (in nm) and Oscillator Strengths (f , in Parentheses), Computed in Solution, for the *cis*-[Ru(L)₂(NCS)₂] (L = bpy, dcbpy) Complexes^a

	bpy	dcbpyH ₂	dcbpy ²⁻	assignment
band I	546 (0.027)	651 (0.046)	542 (0.034)	MLCT
	467 (0.132)	540 (0.163)	468 (0.185)	
	447 (0.040)	467 (0.118)	442 (0.043)	
		447 (0.116)	425 (0.060)	
band II	384 (0.024)	416 (0.022)	380 (0.033)	MLCT + LBCT
		354 (0.049)	413 (0.042)	
		412 (0.028)	371 (0.061)	
		363 (0.073)	357 (0.068)	
			354 (0.021)	
			350 (0.022)	
			344 (0.072)	
			343 (0.020)	

^a Only transitions with $f \geq 0.02$ are reported.

From a quantitative point of view, for all sulfur-bearing compounds, the computed data are in excellent agreement with the available experimental data for both band positions and relative intensity. This confirms, once again, the good performance of TD-DFT and of the PBE0 functional for the description of valence excitations in organometallic complexes.

To clearly distinguish the different ligands effects on UV–vis spectra, we first report on the carboxylic groups influence, comparing the data obtained only for the S-based complexes, summed up in Tables 3 and 4. Next, the discussion will be devoted to the analysis of the effect of the NCX ligand when X is varied from S to Se or Te only in the case of the *cis*-[Ru-

TABLE 4: Computed and Experimental Absorption Maxima Energies, Band Separation ($\Delta E(I-II)$ in nm), and Band Shifts upon Deprotonation ($\Delta(\text{dcbpyH}_2/\text{dcbpy}^{2-})$ in nm) of *cis*-[Ru(L)₂(NCS)₂] (L = bpy, dcbpy) Species (B3LYP Data Are Taken from Reference 32; PBE0 Data Computed in Solution)

	bpy		dcbpyH ₂		dcbpy ²⁻			$\Delta(\text{dcbpyH}_2/\text{dcbpy}^{2-})$			assignment
	PBE0	PBE0	B3LYP	exp. ^a	PBE0	B3LYP	exp. ^b	PBE0	B3LYP	exp. ^a	
band I	500	536	481	521	492	494	500	-44	+13	-21	MLCT
band II	370	390	385	390	361	376	372	-29	-9	-18	MLCT + LBCT
$\Delta E(I-II)$	130	146	96	131	131	118	128				

^a See ref 42. ^b See ref 35.

TABLE 5: Vertical Excitation Energies (in nm) and Oscillator Strengths (f , in Parentheses) Computed in Solution for the *cis*-[Ru(dcbpy)₂(NCX)₂]⁴⁺ Complexes^a

	S		Se		Te		assignment
	abs. max	transitions	abs. max	transitions	abs. max	transitions	
band I	492	542 (0.034) 533 (0.014) 468 (0.185) 442 (0.043)	493	539 (0.034) 529 (0.015) 471 (0.162) 447 (0.050)	501	540 (0.033) 530 (0.017) 482 (0.109) 463 (0.048)	MLCT
band II	361	380 (0.033) 373 (0.078) 371 (0.061) 357 (0.068) 354 (0.021) 350 (0.022) 344 (0.072) 343 (0.020) 341 (0.020)	375	380 (0.027) 373 (0.046) 371 (0.064)	402	414 (0.015) 383 (0.014) 380 (0.020)	MLCT + LBCT (NCX → π^* and COO ⁻ → π^*)

^a Corresponding absorption maxima are given in all cases; only transitions with $f \geq 0.01$ are reported in the table.

(dcbpy)₂(NCX)₂]⁴⁺, the results and overall trends being similar for the corresponding *cis*-[Ru(bpy)₂(NCX)₂] and *cis*-[Ru(dcbpyH₂)₂(NCX)₂] systems. All data are summarized in Table 5.

When going from the bpy ligand to its protonated or deprotonated carboxylated forms, very similar transitions are computed, both in position and in intensity (Table 3). Furthermore, the separation between the bands remains almost constant (Table 4). This fact justifies the use of the *cis*-[Ru(bpy)₂(NCS)₂] complex as a model to compute the UV-vis properties of the N3 dye, as previously reported in the literature.²¹ It must be also pointed out that, from a computational point of view, the PBE0 functional allows for a better description of the spectra with respect to the more popular hybrid B3LYP approach, the maximal deviation between computed and experimental band I position being of only 15 nm. This level of accuracy already allowed for the use of the current protocol (PBE0-TD-DFT) for the prediction of the spectral properties of a new photoactive species.^{10,41}

Fine effects due to deprotonation of N3 can be also evidenced from our calculations. In particular, the experimentally observed acidichromic effect shown by the N3 complex (L = dcbpyH₂ and dcbpy²⁻),⁴² that is, the blue-shift observed when going from the N3 dye to its fully deprotonated form, is well reproduced as shown comparing the computed and experimental Δ values reported in Table 4. It is worth mentioning that both bands are blue-shifted and show similar absorption intensities when using PBE0 in agreement with the experimental findings³⁴ but in contrast to a recent B3LYP investigation³² where a red-shift of the first band was computed.

Finally, we note that, in the energy range considered, no transitions involving carboxylic moieties could be found. This is in line with previous theoretical works,^{21,40} carboxylic groups operating in transitions of higher energies.

If one now analyzed the effect of the chalcogenide tuning on the spectra, from Table 5, it is clear that band I is practically

insensitive to the nature of the X atom on the NCX moiety. This is fully consistent with the fact that this band corresponds to multiple $t_{2g}-\pi^*/t_{2g}-\pi$ to π^* -bpy levels, thus not affected by the X tuning. However, a significant effect is observed for band II, showing a strong red-shift when going from X = S to X = Se and Te. This shift is, once again, easily related to the nature of transitions involved in this absorption band, which are both of the MLCT and LBCT types. More precisely, LBCT transitions concern nonbonding NCX and π^* -bpy levels, these former being largely affected by the tuning of X, as already mentioned in section 3. In addition, it is worth mentioning that, while the S- and Se-based compounds do show similar absorption intensities, in case of the Te-based complex, absorption intensities are much lower than in the former cases, at least by a factor of 2, thus making this system less suitable for photovoltaic applications.

5. Conclusion

A computational protocol based on the use of DFT and TD-DFT in conjunction with the hybrid PBE0 functional has been applied to study the ground- and excited-state properties of a series of nine compounds derived from the N3 dye used in hybrid photovoltaic cells. Besides the remarkable agreement with the available experimental data, which confirms the predictive properties of the computational approach, our results allow us to better clarify the role of the functionalization of the ligands with respect to the absorption properties of the dye.

In particular, from our calculations, the following conclusions can be drawn:

- (i) no significant structural changes between the nine systems can be evidenced, in particular for what concerns the Ru coordination sphere;
- (ii) the carboxyl groups on the bpy moieties do not alter the absorption properties of the compound and serve only to anchor the dye to the surface. A small acidichromic shift, experimentally

evidenced, is fully recovered by the calculations and mainly due to the gap opening upon deprotonation. Indeed, one can safely assume that the absorption properties of the dye are well reproduced using a model where the dcby ligands are substituted by the simpler bpy ones;

(iii) from the point of view of the electronic structure, changing the chalcogen (X) within the ambidentate NCX ligand from S to Se or Te slightly stabilizes the LUMOs and destabilizes the HOMOs, no matter if bpy or dcby ligands are taken into account;

(iv) macroscopically, the overall effect of tuning the chalcogen (X) is to red-shift both absorption bands of N3 (that is, band I and band II), the effect being sizable only in the latter case. This is not surprising because, while the first one (around 500 nm) corresponds to multiple MLCT transitions, the second one (around 370 nm) has a mixed character, deriving from both MLCT and LBCT transitions. In this latter case, transitions involve MO centered on the NCX fragment, and, as a consequence, the second band is affected by changing X, showing a strong red-shift when going from X = S to Se or Te;

(v) a loss of intensity of the absorption bands is computed when passing from S to Se or Te, the effect being more marked for the tellurium derivatives;

(vi) from a methodological point of view, the PBE0 functional seems to correct the well-known overestimated B3LYP picture of Ru–N distances in these types of complexes and allows for the recovering of acidichromic shift for both bands contrary to the B3LYP functional.

In conclusion, with respect to potential future experimental applications of the investigated complexes, the *cis*-Ru(dcby₂)-(NCS₂)₂ one may appear as a good candidate to enhance, although only slightly, the response of the N3 dye to solar light. Indeed, this latter complex is a good compromise between a red-shift of both bands and reasonable intensity loss when compared to the corresponding sulfur and tellurium compounds.

Acknowledgment. The “Institut de Développement et Ressources en Informatique Scientifique” (IDRIS, Orsay) is acknowledged for the allocation of computer time (Project 072115). M.R. thanks the Université des Sciences et de la Technologie Houari Boumediene for a visiting grant to the ENSCP.

References and Notes

- Hagfeldt, A.; Grätzel, M. *Chem. Rev.* **1995**, *95*, 49.
- O'Regan, B.; Grätzel, M. *Nature* **1991**, *353*, 737.
- Hagfeldt, A.; Grätzel, M. *Acc. Chem. Res.* **2000**, *33*, 269.
- Kalyanasundaram, K.; Grätzel, M. *Coord. Chem. Rev.* **1998**, *177*, 347.
- Nazeeruddin, M. K.; Kay, A.; Rodicio, I.; Humphry-Baker, R.; Müller, E.; Liska, P.; Vlachopoulos, N.; Grätzel, M. *J. Am. Chem. Soc.* **1993**, *115*, 6382.
- Grätzel, M. *J. Photochem. Photobiol., A* **2004**, *164*, 3.
- Kohle, S.; Ruile Grätzel, M. *Inorg. Chem.* **1996**, *35*, 4779.
- Nazeeruddin, M. K.; Péchy, P.; Renouard, T.; Zakeeruddin, S. M.; Humphry-Baker, R.; Comte, P.; Liska, P.; Cevey, L.; Costa, E.; Shklover, V.; Spiccia, L.; Deacon, G. B.; Bignozzi, C. A.; Grätzel, M. *J. Am. Chem. Soc.* **2001**, *123*, 1613.
- Boschloo, G.; Lindström, J.; Magnusson, E.; Holmberg, A.; Hagfeldt, A. *J. Photochem. Photobiol., A* **2002**, *148*, 11.
- Ciofini, I.; Lainé, P. P.; Bedioui, F.; Adamo, C. *J. Am. Chem. Soc.* **2004**, *126*, 10763.
- Lainé, P. P.; Ciofini, I.; Ochsenein, P.; Amouyal, E.; Adamo, C.; Bedioui, F. *Chem.-Eur. J.* **2005**, *11*, 3711.
- Ciofini, I.; Lainé, P. P.; Bedioui, F.; Daul, C. A.; Adamo, C. *C. R. Acad. Sci.* **2006**, *9*, 226.
- Ciofini, I. *Theor. Chem. Acc.* **2006**, *116*, 219.
- Lainé, P. P.; Loiseau, F.; Campagna, S.; Ciofini, I.; Adamo, C. *Inorg. Chem.* **2006**, *45*, 5538.
- Labat, F.; Baranek, P.; Domain, C.; Minot, C.; Adamo, C. *J. Chem. Phys.* **2007**, *126*, 154703.
- Ciofini, I.; Zamboni, M.; Lainé, P. P.; Marvaud, V.; Daul, C. A.; Adamo, C. *Chem.-Eur. J.* **2007**, *13*, 5360.
- Jacquemin, D.; Perpète, E. A.; Frisch, M. J.; Scalmani, G.; Ciofini, I.; Adamo, C. *Chem. Phys. Lett.* **2006**, *421*, 272.
- Jacquemin, D.; Perpète, E. A.; Scalmani, G.; Frisch, M. J.; Assfeld, X.; Ciofini, I.; Adamo, C. *J. Chem. Phys.* **2006**, *125*, 164324.
- Ciofini, I.; Adamo, C. *J. Phys. Chem. A* **2007**, *111*, 5549.
- Miertus, S.; Scrocco, E.; Tomasi, J. *Chem. Phys.* **1981**, *55*, 117.
- Guillemoles, J. F.; Barone, V.; Joubert, L.; Adamo, C. *J. Phys. Chem. A* **2002**, *106*, 11354.
- Ciofini, I.; Daul, C.; Adamo, C. *J. Phys. Chem. A* **2003**, *107*, 11182–11190.
- Frisch, M. J.; Trucks, G. W.; Schlegel, H. B.; Scuseria, G. E.; Robb, M. A.; Cheeseman, J. R.; Montgomery, J. A.; Vreven, T., Jr.; Kudin, K. N.; Burant, J. C.; Millam, J. M.; Iyengar, S. S.; Tomasi, J.; Barone, V.; Mennucci, B.; Cossi, M.; Scalmani, G.; Rega, N.; Petersson, G. A.; Nakatsuji, H.; Hada, M.; Ehara, M.; Toyota, K.; Fukuda, R.; Hasegawa, J.; Ishida, M.; Nakajima, T.; Honda, Y.; Kitao, O.; Nakai, H.; Klene, M.; Li, X.; Knox, J. E.; Hratchian, H. P.; Cross, J. B.; Adamo, C.; Jaramillo, J.; Gomperts, R.; Stratmann, R. E.; Yazyev, O.; Austin, A. J.; Cammi, R.; Pomelli, C.; Ochterski, J. W.; Ayala, P. Y.; Morokuma, K.; Voth, G. A.; Salvador, P.; Dannenberg, J. J.; Zakrzewski, V. G.; Dapprich, S.; Daniels, A. D.; Strain, M. C.; Farkas, O.; Malick, D. K.; Rabuck, A. D.; Raghavachari, K.; Foresman, J. B.; Ortiz, J. V.; Cui, Q.; Baboul, A. G.; Clifford, S.; Cioslowski, J.; Stefanov, B. B.; Liu, G.; Liashenko, A.; Piskorz, P.; Komaromi, I.; Martin, R. L.; Fox, D. J.; Keith, T.; Al-Laham, M. A.; Peng, C. Y.; Nanayakkara, A.; Challacombe, M.; Gill, P. M. W.; Johnson, B.; Chen, W.; Wong, M. W.; Gonzalez, C.; Pople, J. A. *Gaussian 03*, revision A.1; Gaussian, Inc.: Pittsburgh, PA, 2003.
- Adamo, C.; Barone, V. *J. Chem. Phys.* **1999**, *110*, 6158.
- Perdew, J. P.; Burke, K.; Ernzerhof, M. *Phys. Rev. Lett.* **1996**, *77*, 3865.
- Adamo, C.; Cossi, M.; Rega, N.; Barone, V. *Theoretical Biochemistry-Processes and Properties of Biological Systems*; Elsevier Science: New York, 2001; pp 467–538.
- Hay, P. J.; Wadt, W. R. *J. Chem. Phys.* **1985**, *82*, 299.
- Hay, P. J.; Wadt, W. R. *J. Chem. Phys.* **1985**, *82*, 270.
- Gross, E. U. K.; Dobson, J. F.; Petersilka, M. In *Density Functional Theory II*; Nalewajski, R. F., Ed.; Springer: Heidelberg, 1996.
- Cossi, M.; Barone, V.; Cammi, R.; Tomasi, J. *Chem. Phys. Lett.* **1996**, *255*, 327.
- Herber, R. H.; Guijuan Nan; Potenza, J. A.; Schugar, H. J.; Bino, A. *Inorg. Chem.* **1989**, *28*, 938.
- De Angelis, F.; Fantacci, S.; Selloni, A. *Chem. Phys. Lett.* **2004**, *389*, 204.
- Shklover, V.; Ovchinnikov, Y. E.; Braginsky, L. S.; Zakeeruddin, S. M.; Graetzel, M. *Chem. Mater.* **1998**, *10*, 2533.
- Sauve, G.; Cass, M. E.; Coia, G.; Doig, S. J.; Lauermaun, I.; Pomykal, K. E.; Lewis, N. S. *J. Phys. Chem. B* **2000**, *104*, 6821.
- Shklover, V.; Nazeeruddin, M. K.; Zakeeruddin, S. M.; Barbé, C.; Kay, A.; Haibach, T.; Steurer, W.; Hermann, R.; Nissen, H. U.; Grätzel, M. *Chem. Mater.* **1997**, *9*, 430.
- Lundqvist, M. J.; Nilsing, M.; Lunell, S.; Åkermark, B.; Persson P. *J. Phys. Chem. B* **2006**, *110*, 20513.
- Gorelsky, S. I.; Lever, A. B. P. *J. Organomet. Chem.* **2001**, *635*, 187.
- Zhou, X.; Ren, A. M.; Feng, J. K. *J. Organomet. Chem.* **2005**, *690*, 338.
- Zheng, K. C.; Wang, J. P.; Peng, W. L.; Liu, X. W.; Yun, F. C. *J. Mol. Struct. (THEOCHEM)* **2002**, *582*, 1.
- Labat, F.; Lainé, P. P.; Ciofini, I.; Adamo, C. *Chem. Phys. Lett.* **2006**, *417*, 445.
- Ciofini, I.; Lainé, P. P.; Adamo, C., work in progress.
- Nazeeruddin, M. K.; Zakeeruddin, S. M.; Humphry-Baker, R.; Jirousek, M.; Liska, P.; Vlachopoulos, N.; Shklover, V.; Fischer, C.-H.; Grätzel, M. *Inorg. Chem.* **1999**, *38*, 6298.